



City Research Online

City, University of London Institutional Repository

Citation: Stefanitsis, D., Strotos, G., Nikolopoulos, N. & Gavaises, M. (2019). Numerical investigation of the aerodynamic breakup of a parallel moving droplet cluster. *International Journal of Multiphase Flow*, 121, 103123. doi: 10.1016/j.ijmultiphaseflow.2019.103123

This is the preprint version of the paper.

This version of the publication may differ from the final published version.

Permanent repository link: <https://openaccess.city.ac.uk/id/eprint/22918/>

Link to published version: <https://doi.org/10.1016/j.ijmultiphaseflow.2019.103123>

Copyright: City Research Online aims to make research outputs of City, University of London available to a wider audience. Copyright and Moral Rights remain with the author(s) and/or copyright holders. URLs from City Research Online may be freely distributed and linked to.

Reuse: Copies of full items can be used for personal research or study, educational, or not-for-profit purposes without prior permission or charge. Provided that the authors, title and full bibliographic details are credited, a hyperlink and/or URL is given for the original metadata page and the content is not changed in any way.

City Research Online:

<http://openaccess.city.ac.uk/>

publications@city.ac.uk

Numerical investigation of the aerodynamic breakup of a parallel moving droplet cluster

Affiliations

Dionisis Stefanitsis^{*1,2}, George Strotos³, Nikolaos Nikolopoulos¹, Manolis Gavaises²

¹Centre for Research and Technology Hellas/Chemical Process and Energy Resources Institute (CERTH/CPERI), Egialeias 52, Marousi, Greece

²City University London, School of Engineering and Mathematical Sciences, Northampton Square, EC1V 0HB London, UK

³Technological Educational Institute of Thessaly, Mechanical Engineering Department, 41110 Larissa, Greece

*Corresponding author: stefanitsis@certh.gr

gstrot@teilar.gr, n.nikolopoulos@certh.gr, M.Gavaises@city.ac.uk

Abstract

The present work examines numerically the aerodynamic breakup of a cluster of Diesel droplets moving in parallel with respect to the gas flow. Two- and three-dimensional simulations of the incompressible Navier-Stokes equations together with the VOF method are performed for Weber (We) numbers in the range of 5 up to 60 and non-dimensional distance between the droplets (H/D_0) ranging from 1.25 to 20. The numerical results indicate that the proximity of droplets affects their breakup for distances $H/D_0 \leq 5$. For low droplet proximity distances ($H/D_0 \leq 2.5$), the droplets experience the so-called shuttlecock breakup mode, which has been also identified for droplets in tandem formations in a previous authors' work and is characterized by an oblique peripheral stretching of the droplet. With decreasing H/D_0 the breakup initiation time decreases, while the drag coefficient increases relative to that of isolated droplets. When the distance between the droplets is low enough ($H/D_0 < 1.5$), this can result in critical We number, i.e. minimum We number leading to breakup, lower than that of an isolated droplet at the same conditions.

Keywords

Cluster droplet breakup; Diesel; drag coefficient; breakup time; critical We .

Nomenclature

Roman symbols

B	Average dimensionless deformation rate [-]
C_d	Drag coefficient [-]
D	Droplet diameter [m]
D_{cr}	Cross-stream droplet deformation [m]
D_{str}	Streamwise droplet deformation [m]
H	Cross-stream distance between droplet centres [m]
L	Streamwise distance between droplet centres [m]
N	Viscosity ratio [-]

U	Velocity [m/s]
V_{cell}	Volume of cell [m ³]
We	Weber number [-]

Greek symbols

α	Liquid volume fraction [-]
ϵ	Density ratio [-]
μ	Dynamic viscosity [kg/(m·s)]
ρ	Density [kg/m ³]
σ	Surface tension [N/m]

n_{cells}	Number of computational cells [-]
Oh	Ohnesorge number [-]
P	Pressure [Pa]
Re	Reynolds number [-]
S	Droplet surface area [m ²]
T	Temperature [K]
t	Time [s]
t^*	Non-dimensional time [-]
t_{br}	Breakup initiation time [s]
t_{sh}	Shear breakup timescale [s]

Subscripts

0	Initial
cl	Cluster
cr	Critical
d	Droplet
g	Gas phase
is	Isolated droplet
L	Liquid phase
max	Maximum
rel	Relative

33

34 1 Introduction

35 Droplet deformation and eventually breakup is encountered in various systems and applications [1].
 36 The non-dimensional numbers usually utilised for classifying the breakup outcome of isolated droplets
 37 are the Weber (We), Ohnesorge (Oh) and Reynolds (Re) numbers as well as the density (ε) and viscosity
 38 ratios (N) of the two phases [2]; these are defined as:

39

$$We = \frac{\rho_g U_{rel,0}^2 D_0}{\sigma} \quad Oh = \frac{\mu_L}{\sqrt{\rho_L \sigma D_0}} \quad Re = \frac{\rho_g U_{rel,0} D_0}{\mu_g} \quad \varepsilon = \frac{\rho_L}{\rho_g} \quad N = \frac{\mu_L}{\mu_g} \quad (1)$$

40

41 The breakup timescale can be also approximated by the non-dimensional correlation proposed by
 42 Nicholls and Ranger [3]:

43

$$t_{sh} = \frac{D_0}{U_{rel,0}} \sqrt{\varepsilon} \quad (2)$$

44

45 The aerodynamic breakup of isolated droplets has been thoroughly investigated (see for example [2]
 46 among many others); more recently the breakup of droplets in tandem formations has been also
 47 reported [4-6]. On the other hand, not much focus has been paid to the breakup of droplets moving in
 48 parallel with respect to the surrounding air; such collective droplet cluster motions can be considered
 49 more representative for the conditions typically realised in fuel sprays consisting of a large number of
 50 droplets [1]. In these formations apart from the non-dimensional streamwise distance between the
 51 droplets (L/D_0), also the cross-stream one (H/D_0) can be speculate to play a role; the L and H here
 52 correspond to distances between the droplet centres.

53 Regarding the hydrodynamic interaction between rigid particles, the experimental works of [7, 8]
 54 examined two particles exposed in parallel to a uniform flow of water, with non-dimensional distances
 55 between them (H/D_0) ranging from 1 up to 2.5 and Re number equal to 5,000. They studied mainly the
 56 flow around the particles and concluded that for $H/D_0=1$ (particles are in contact) the particles act as
 57 a rigid bluff body, while for $H/D_0 \geq 2$ the interaction between the shedding vortices is minimized as well
 58 as the effect of the jet-like flow occurring through them. Numerical studies of similar particle
 59 arrangements were performed by Folkersma et al. [9], Tsuji et al. [10], Ardekani et al. [11], Pahl et al.
 60 [12], Yoon and Yang [13] and by Jadoon [14]. The Re numbers examined range from $5 \cdot 10^{-7}$ up to 600,
 61 while the non-dimensional distance between the particles are in the range of 1 up to 23. These studies

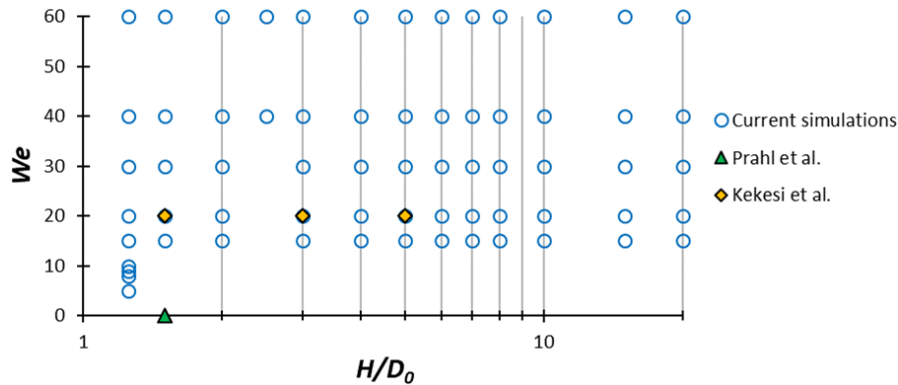
62 focus mainly on the estimation of the force coefficients (drag, lift and pressure); it is generally
63 concluded that the drag coefficient is higher for the parallel particle motion configuration compared
64 to that of an isolated particle.

65 Turning now to studies referring to the parallel motion of droplets as opposed to solid particles, Temkin
66 and Ecker [5] performed experiments with streams of water droplets at Re numbers in the range of
67 130 up to 600 and H/D_0 ranging from 3 up to 6 and streamwise distance between them L/D_0 from 1.5
68 up to 11. They observed that the wake of a droplet affects the drag coefficient of the trailing droplets
69 that lie within a parabolic shape of $15D_0$ length and $1D_0$ width. Connon and Dunn-Rankin [15] studied
70 experimentally the behavior of an isolated water droplet displaced radially from a droplet stream, and
71 concluded that the droplet stream influences its surroundings for $H/D_0 \leq 15$ and $L/D_0 \leq 15$. Later, Zhao et
72 al. [16] investigated experimentally the aerodynamic breakup of two water droplets arranged at
73 various configurations with streamwise and cross-stream non-dimensional distances less than 3, while
74 the Re number was equal to 2680 and the We equal to 12.3. They identified four breakup modes: i)
75 coalescence, ii) puncture, iii) side-by-side and iv) no direct contact, and concluded that the fastest
76 mode is the side-by-side, in which the droplets deform into a disk-like shape with their edges touching
77 before the breakup occurs. This breakup mode is encountered for $H/D_0 \leq 2$.

78 Numerical simulations with droplets and solid spheres were performed by Kim and coworkers in [17,
79 18] for $Re=100$ and H/D_0 ranging from 1.5 up to 25. They found that for $H/D_0 < 9$ the drag coefficient of
80 the droplets is higher than that of an isolated droplet at the same conditions. Prahl et al. [19]
81 investigated numerically with the Volume of Fluid (VOF) method the interaction of two droplets
82 exposed in a uniform flow of $Re=100$ and $We=0.1$ and 1. The streamwise distance between the droplets
83 ranged from 1.5 up to 6, while the cross-stream one was equal to 1.5. It was found that for the parallel
84 arrangement, the droplets experience higher drag force compared to the isolated droplet and also a
85 weak attraction. Recently, Kekesi et al. [6] studied numerically using the VOF method the breakup of
86 two liquid droplets arranged at various positions from tandem up to parallel, with $We=20$, $Re=20$ and
87 50, and L/D_0 and H/D_0 ranging from 1.5 up to 5. Three scenarios were identified for the breakup of the
88 droplets: i) they collide and merge, ii) the secondary drop shoot through the primary drop and iii) the
89 two drops behave independently. Finally, they found that for certain parallel configurations the
90 breakup time is shorter than that of an isolated droplet. This was attributed to the increased velocity
91 in the gap between the droplets, which results in enhanced shear at the droplet periphery.

92 The aforementioned numerical studies examined the breakup of two droplets moving in parallel to the
93 air flow, while the current work investigates, for the first time, the breakup of a droplet inside a cluster
94 of droplets; this can be considered as a typical droplet appearing at the inner part of a spray. More
95 specifically, four droplets are simulated, or equivalently one droplet with symmetry boundary
96 conditions (the equivalence of these configurations is proved in section 2.1), which represent an
97 infinite cluster with the use of symmetry boundary conditions, as shown in Figure 2. Qualitative results
98 are presented for the temporal evolution of droplet shape as well the breakup mode. In addition, a
99 parametric study is performed with 2-D axisymmetric simulations for We and H/D_0 numbers as shown
100 in Figure 1, where the previous numerical studies are presented as well. As it can be seen, a big portion
101 of the map has not been investigated so far. The 2-D axisymmetric simulations are performed with a
102 single droplet, while the effect of other droplets in their proximity is simulated using symmetry
103 boundary conditions. Results are presented for the effect of H/D_0 on the breakup mode, maximum

104 surface area, critical We number (minimum We number leading to breakup), breakup initiation time
 105 and drag coefficient.
 106



107
 108 Figure 1. Examined We and H/D_0 numbers of the current and previous numerical studies.
 109

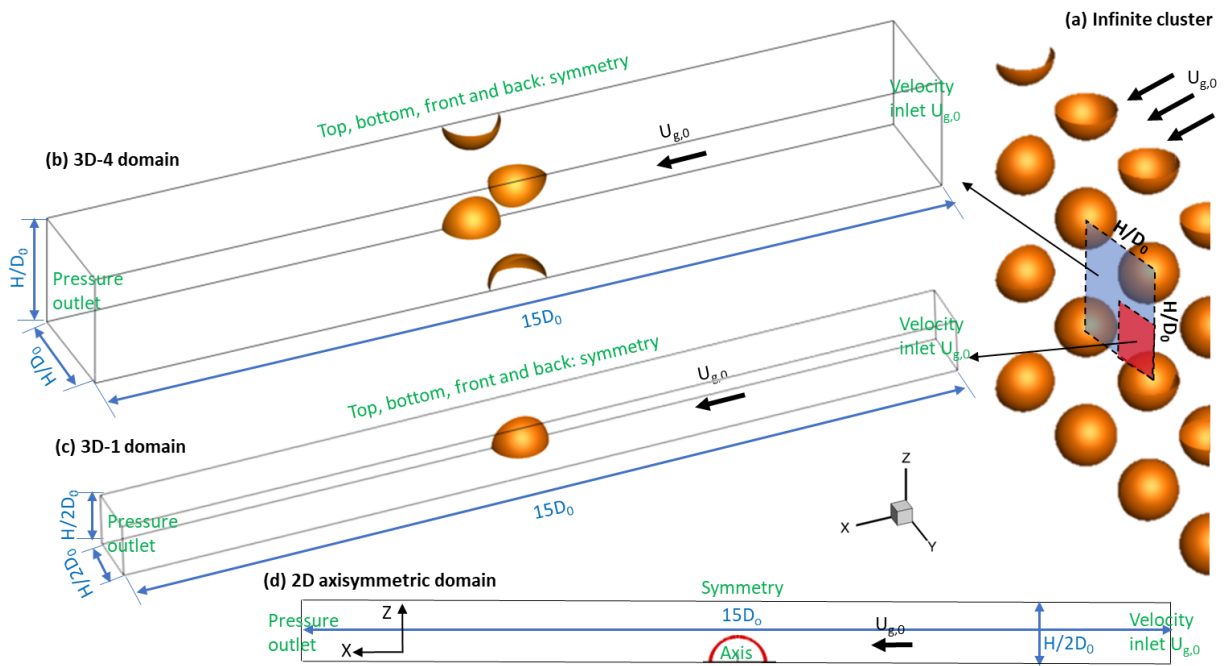
110 The paper is structured as follows: initially, the computational setup and examined conditions are
 111 presented, followed by a section presenting the qualitative results as well as the results of the
 112 parametric study. Finally, the main conclusions are summarized in the last section of the paper.
 113

114 2 Computational setup and examined conditions

115 The numerical model for the parallel droplet cluster motion and breakup solves the Navier-Stokes
 116 equations coupled with the Volume of Fluid (VOF) methodology [20] for tracking the interface between
 117 the liquid droplets and the surrounding gas. In order to model surface tension, the Continuum Surface
 118 Stress (CSS) model of [21] is utilized. Two-dimensional (2-D) axisymmetric and three-dimensional (3-
 119 D) simulations are performed with the commercial CFD tool ANSYS FLUENT v16 [22] along with the use
 120 of various User Defined Functions (UDFs); these account for the following: i) adaptive local grid
 121 refinement technique around the liquid-gas interface [23], ii) adaptive time-step scheme for the
 122 implicit VOF solver based on the velocity at the droplet interface [24], and iii) moving mesh technique
 123 based on the average velocity of the droplets. The CFD model has been developed and validated in
 124 previous works of the authors for a number of applications; among them are the free fall of a droplet
 125 [23], the droplet impingement on a flat wall [25] or a spherical particle [26-28], the aerodynamic
 126 droplet breakup [4, 24, 29-35] and the droplet evaporation [24, 31, 36]. It should be noted that the
 127 extension of the model validation for the case of droplet clusters is not possible since, to the author's
 128 best of knowledge, there are no experimental studies in the literature with droplet clusters, only a few
 129 featuring two droplets [5, 15, 16]. However, even with two droplets a 3D simulation would require
 130 approximately twice more computational resources than the simulation of four droplet quarters (3D-
 131 4 domain of Figure 2), in terms of CPU-hours. For this reason, and since the physical process is the
 132 same between the breakup of one and more droplets, we have assumed that the model is considered
 133 validated using only the case of the isolated droplet.

134 Figure 2 presents an infinite cluster of droplets arranged parallel to the air flow along with the
 135 computational domains utilized in the current work for its simulation: i) a 3-D domain with four droplet
 136 quarters (abbreviated as 3D-4), ii) a 3-D domain of a single droplet quarter (abbreviated as 3D-1), and
 137 iii) a 2-D axisymmetric domain. In all cases symmetry boundary conditions are utilized to reflect the
 138 presence of surrounding droplets. In the following section (2.1) it is shown that the two examined 3-D

139 configurations are equivalent, since they give identical results for a simulation at the same conditions.
 140 On the other hand, for the case of the 2D axisymmetric simulations, the adoption of a symmetry
 141 boundary condition does not strictly reflect the effect of the neighbour droplets at a 45° direction
 142 (diagonal). However, the results using the 2-D domain are close to those of the 3-D simulations, even
 143 for very low values of $H/D_0 (=2)$ (see section 2.1). For this reason, the 2D approach is utilized in the
 144 parametric study since it is much more computationally efficient than the other two, therefore making
 145 it possible to simulate the 67 examined cases within a reasonable time.
 146 The droplet is initially stagnant, while air flows from the right boundary forcing it to move and deform.
 147 In Figure 2c and d, the distance measured from the centre of the droplet to the symmetry boundary
 148 conditions is equal to half the distance between the droplets ($H/2D_0$). In the depicted cases of Figure
 149 2 this is equal to 1, and therefore $H/D_0=2$, while for a different H/D_0 the height of the domain should
 150 be adjusted accordingly, resulting in a new computational domain. The computational cells have a
 151 rectangular/hexahedron shape with a base grid resolution equal to 3 cells per radius (cpR), while 6
 152 levels of local grid refinement (or 5 for the 3-D cases) are applied to obtain the desired resolution of
 153 192cpR (or 96cpR for the 3-D) around the liquid-gas interface. The resolution of 96cpR has been found
 154 to be adequate for the simulations of droplet breakup as the average drop velocity, deformation and
 155 breakup initiation time change less than 1% when a finer grid is used. To give an idea about the grid
 156 size, the 3D-4 computational domain utilizes initially approximately 2.5 million cells, which increase up
 157 to 8.7 million at the end of the simulation, due to the use of the adaptive local grid refinement.
 158



159
 160 Figure 2. a) Actual configuration with an infinite cluster of droplets along with the computational domains and
 161 boundary conditions used in the simulations: b) 3D-4 domain, c) 3D-1 domain, and d) 2-D axisymmetric
 162 domain.
 163

164 The simulations have been performed with Diesel fuel as liquid with properties taken from [37], using
 165 a four component surrogate and the PC-SAFT equation of state; a pressure of 40bar and a temperature
 166 of 900K were considered for the estimation of gas properties, while a temperature of 335K was
 167 assumed for the liquid properties. These conditions correspond to those encountered in Diesel engines

168 as presented in Table 1, along with the corresponding references used for their estimation. It should
169 be noted that at such high air temperature, heating and evaporation of the droplets takes also place,
170 but these were neglected in the current work, since its primary scope lies on the investigation of the
171 effect of droplet proximity (similar to our previous work [38]). In view of that, any variations of droplet
172 physical properties with temperature, including that of surface tension, were neglected, as the flow
173 was considered to be isothermal. The justification for this approximation is given using the model of
174 Strotos et al [31] to predict the heating and evaporation of a Diesel droplet in cluster formation with
175 $We=40$ and $H/D_0=2$. The liquid physical properties used are those of Table 1, while the temporal
176 evolution of droplet surface area is calculated based on the CFD simulations instead of the derived
177 equation in [31]. For a typical duration of $t=1.5t_{sh}$, during which the droplet undergoes breakup as
178 shown in Figure 5, less than 1% of the droplet mass has been evaporated, while the mean temperature
179 of the droplet increases by about 8K. This change of liquid temperature results in a decrease to its
180 surface tension and viscosity equal to approximately 3% and 11%, respectively (properties based on
181 [39] and [37], respectively).

182 The resulting non-dimensional numbers from the properties of Table 1 are: $Oh=0.05$, $\varepsilon=51$ and $N=37$.
183 By changing the initial droplet velocity, the obtained We numbers range from 5 up to 60, while the Re
184 number lies in the range of 240 to 832; it should be noted that for an isolated droplet these conditions
185 correspond to the bag and multi-mode regimes. The examined non-dimensional distances measured
186 from the droplet centers (H/D_0) range from 1.25 up to 20, resulting in 69 examined cases (two of which
187 are in 3 dimensions with $We=40$ and $H/D_0=2$) in total (see Figure 1). Finally, 2-D axisymmetric
188 simulations have been performed with an isolated droplet as well, using the same computational
189 domain and conditions, resulting in 10 simulations in total in the range of $We=15-60$. These simulations
190 are utilized in section 3.2 to calculate the quantities of the isolated droplet, which are compared with
191 those of the droplet in a cluster; the quantities of both configurations are functions of the We number.

192
193 Table 1. Representative Diesel engine conditions.

	D_0 (μm)	P (bar)	T_g (K)	μ_g (kg/s·m)	ρ_g (kg/m ³)	T_l (K)	μ_l (kg/m·s)	ρ_l (kg/m ³)	σ (N/m)
Value	50	40	900	4E-05	15.48	335	0.0015	788.6	0.024
Reference	[40]	[41]	[41]	[42]	Ideal gas law	[41]	[37]	[37]	[39]

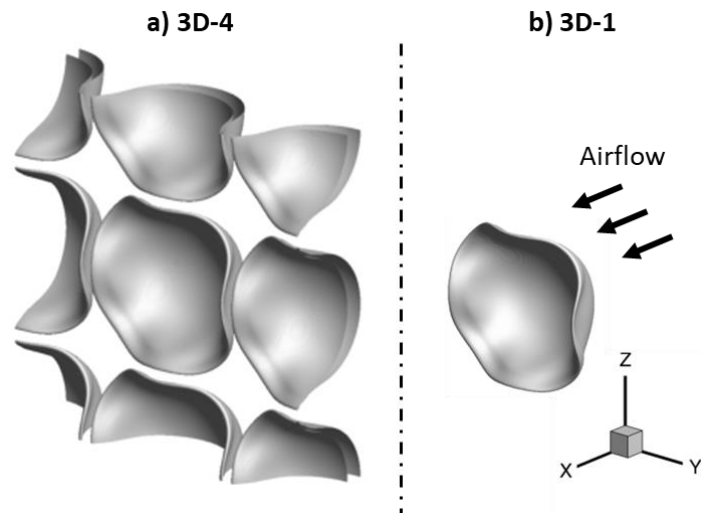
194

195 2.1 Comparison between the computational domains

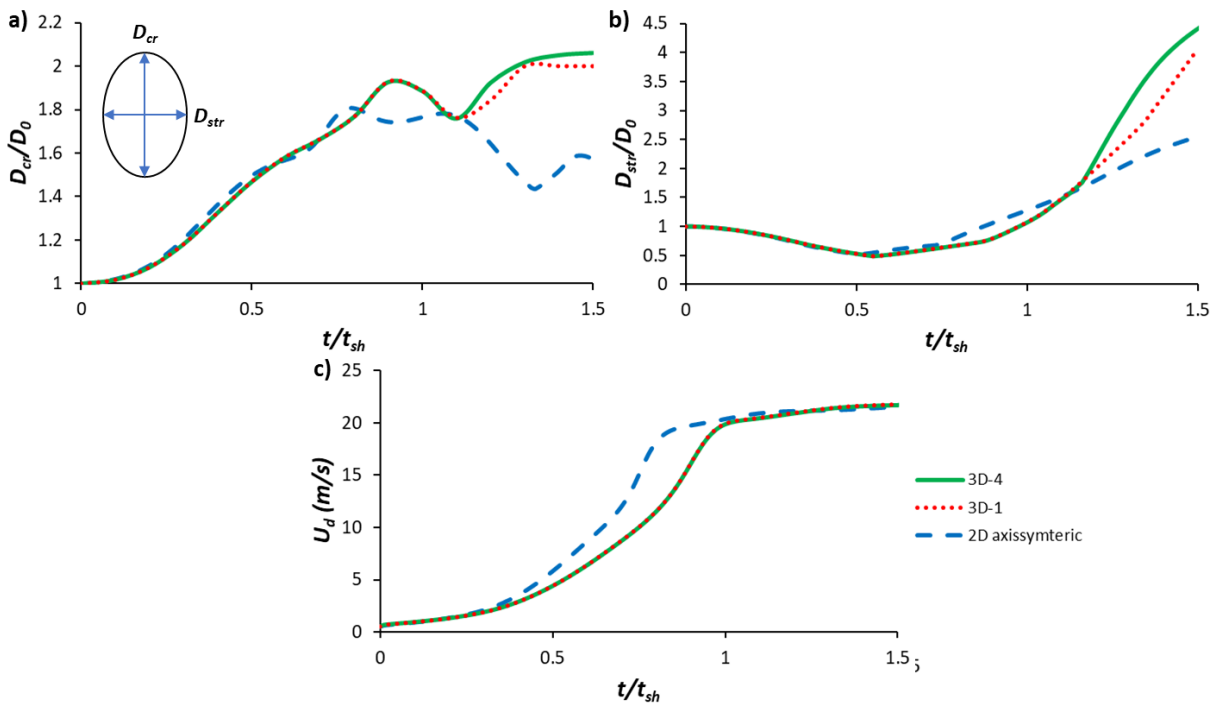
196 Before proceeding to the discussion of the results, a comparison is made between the computational
197 domains of Figure 2 in order to justify their selection for the corresponding simulations. Figure 3
198 presents the temporal evolution of droplets' shape (VOF iso-value of 0.5) as predicted by the
199 simulation of a case with $We=40$ and $H/D_0=2$ using the 3D-4 and 3D-1 computational domains. As it is
200 observed, the droplet shapes of the four droplets are identical between them as also with that of the
201 single droplet (3D-1 domain). This is further justified by looking at Figure 4, which presents the
202 temporal evolution of droplet deformation in both axes (cross-stream and streamwise) as well as the
203 droplet velocity. The results of the 3D-4 and 3D-1 domains are identical for the droplet velocity, while
204 a small deviation is observed for the droplet deformation after $t/t_{sh}=1.1$, which is attributed to the
205 micro-droplets that are detached from the parent droplet. In the following sections, only the results
206 of the 3D-1 configuration are presented for simplicity. It should be noted that the cross-stream
207 deformation in the 3D simulations varies in the Y-Z plane (see Figure 5). For reasons of simplicity, we

208 have assumed that $D_{cr}=0.5*(D_y+D_z)$, without accounting for any disturbances in the diagonal direction
 209 of the Y-Z plane.

210 Turning now to the results of the 2D-axisymmetric simulation, these are presented in Figure 4 as well.
 211 As it can be seen, they are close to those of the 3D simulations for the droplet deformation, while for
 212 the droplet velocity a small deviation is observed, up to approximately $t/t_{sh}=1$. Nevertheless, these
 213 differences are expected to decrease at higher droplet distances H/D_0 , as the droplets in cluster
 214 formation tend to approach the behavior of an isolated droplet. The results of the 2-D axisymmetric
 215 simulations are utilized mainly for the parametric study of this work, since they require approximately
 216 160 times less computational resources than the 3D-1 domain, in terms of CPU-hours.
 217



218
 219 Figure 3. Droplet shape at the time instance of $t/t_{sh}=1$ as predicted by the simulation of a case with $We=40$ and
 220 $H/D_0=2$ using a) the 3D-4 and b) the 3D-1 computational domains.
 221



222

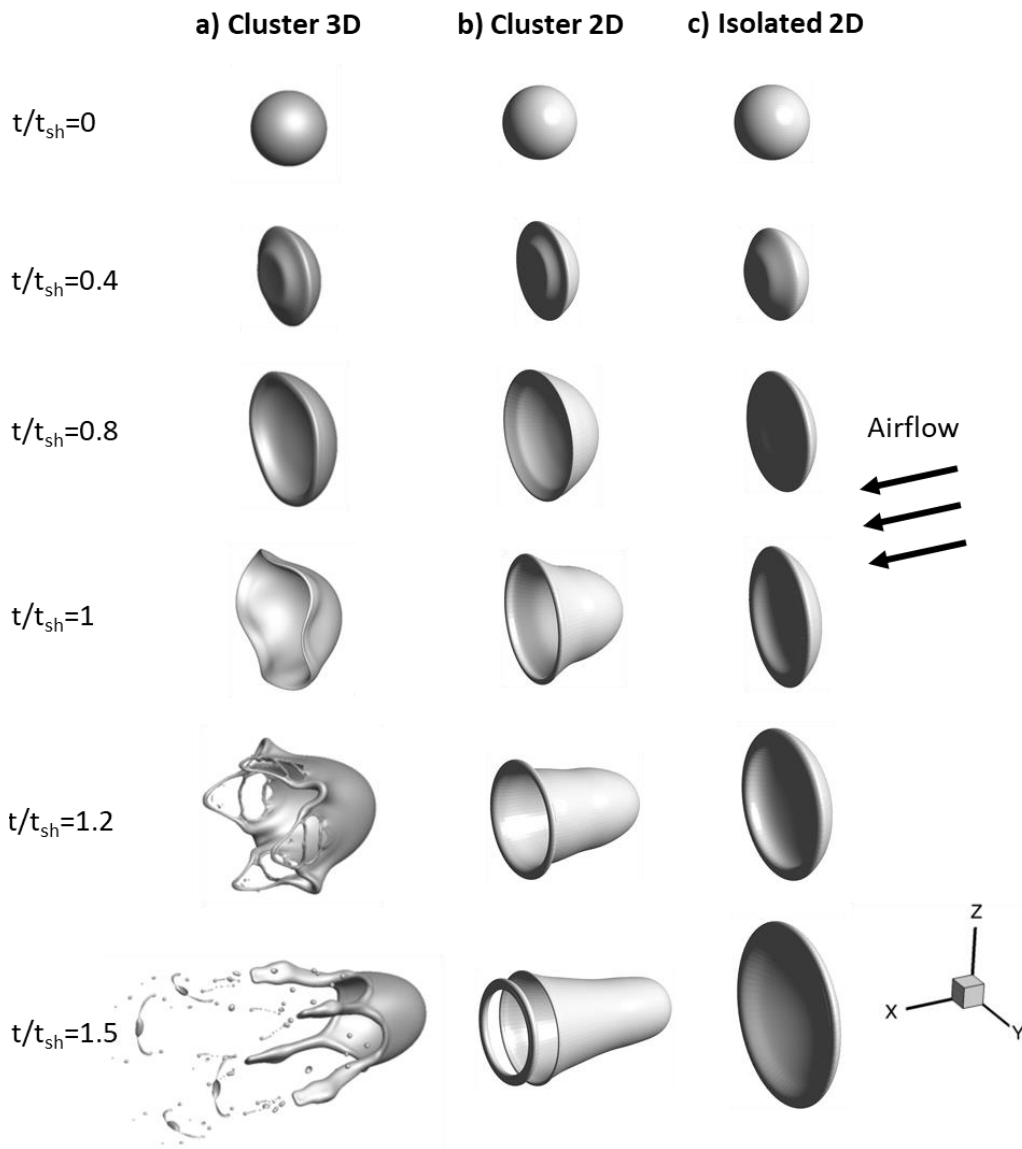
223 Figure 4. Temporal evolution of a) cross-stream droplet deformation, b) streamwise droplet deformation, and
224 c) droplet velocity, as calculated by a simulation with $We=40$ and $H/D_0=2$ using the three computational
225 domains: i) 3D-4, ii) 3D-1 and iii) the 2-D axisymmetric.
226

227 3 Results and discussion

228 3.1 Qualitative results

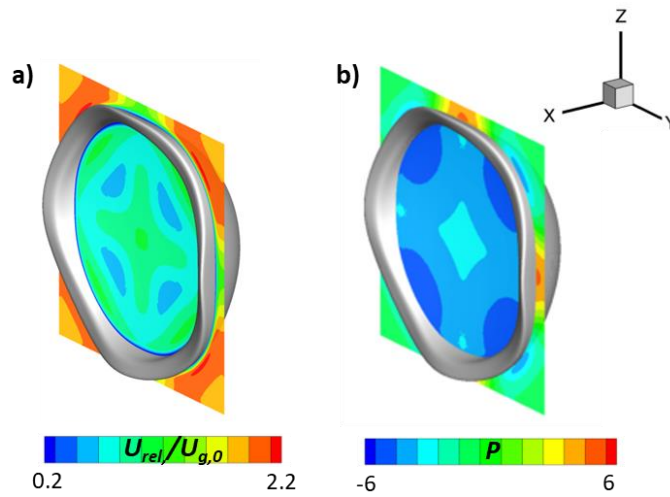
229 Figure 5 illustrates the temporal evolution of droplet shape as predicted both by the 3-D and the 2-D
230 axisymmetric simulations (shape drawn with 3-D rotation around the x-axis) of a case with $We=40$ and
231 $H/D_0=2$, as well as from the simulation of an isolated droplet at the same We number (2-D axisymmetric
232 with 3-D rotation). As it is observed, the droplet in the cluster formation initially deforms into a disk-
233 like shape ($t/t_{sh}=0.4$), followed by a semi-spherical shape ($t/t_{sh}=0.8$); breakup occurs with stripping of
234 liquid from its periphery ($t/t_{sh}=1.5$). This breakup mode is called shuttlecock and has been identified in
235 the authors' previous work for the breakup of droplets in tandem formation [4]; it is characterized by
236 a large streamwise droplet deformation, while most of the liquid volume remains at its core. Turning
237 now to the isolated droplet, it experiences the well-known multi-bag breakup regime, in which the
238 droplet gradually deforms into a disk-like shape followed by the creation of a bag at its periphery (not
239 shown here). In addition, its breakup occurs much slower compared to the cluster arrangement, at
240 approximately $t/t_{sh}=2.3$ compared to $t/t_{sh}=1.4$ (and 1.2 in the 3-D simulation); this observation was also
241 reported in the work of [6].

242 Regarding the comparison between the 2-D and 3-D simulations, they both predict similar droplet
243 shapes up to $t/t_{sh}=0.8$, while after $t/t_{sh}=1$ a deviation is observed. At that time instance, the 3-D
244 simulation predicts a wavy shape for the ring formed around the droplet, as shown in Figure 5 ($t/t_{sh}=1$).
245 This is attributed, on the one hand, to the Kelvin-Helmholtz instabilities [43, 44], and on the other to
246 bigger gap between the droplets in the diagonal direction compared to the vertical one. This causes
247 non-uniform pressure and velocity distributions along the periphery of the droplet, as shown in Figure
248 6, where the Y-Z slices are presented for the dimensionless pressure $((P - P_\infty)/\frac{1}{2}\rho_g U_{g,0}^2)$ and relative
249 velocity ($t/t_{sh}=0.9$). Eventually, at $t/t_{sh}=1.5$ the waves turn into ligaments, since most of the liquid is
250 concentrated at the corners of the droplet rather than its center.
251



252
 253
 254
 255
 256

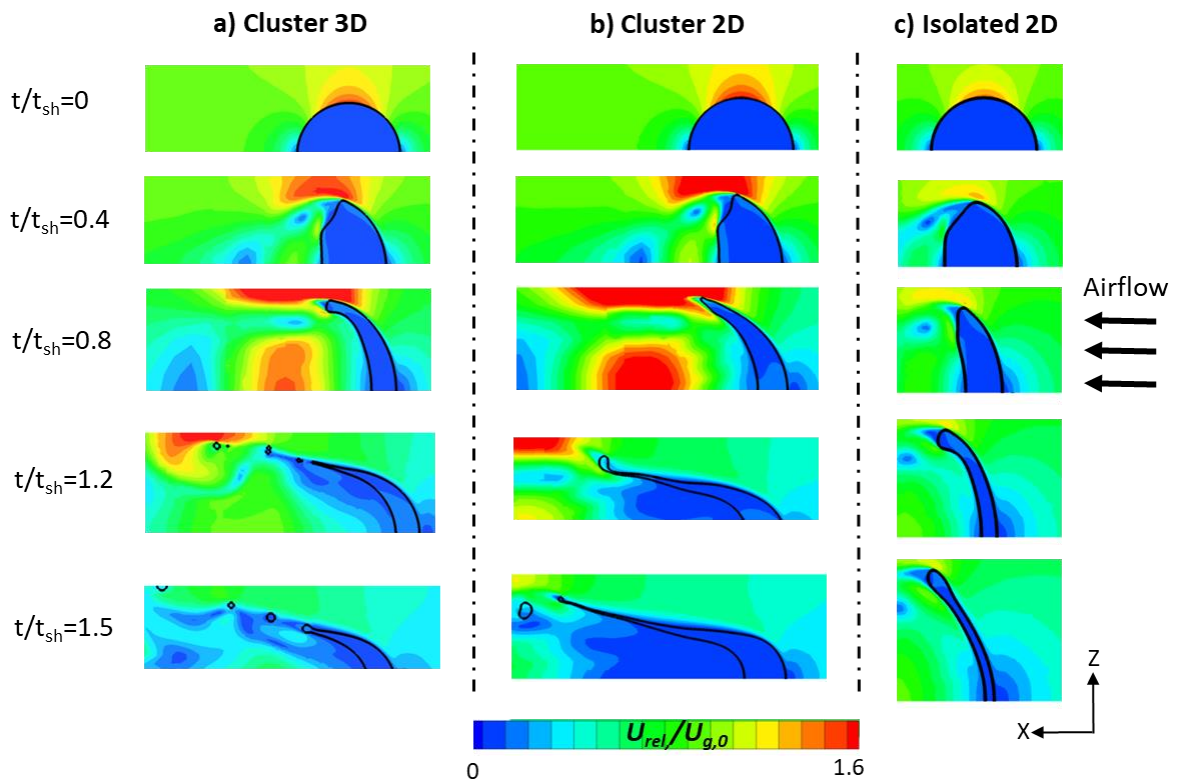
Figure 5. Temporal evolution of droplet shape as predicted by a) the 3-D simulation and b) the 2-D axisymmetric (3-D rotation) of a droplet in a cluster with $H/D_0=2$ and $We=40$, as well as an isolated droplet at the same We number.



257

258 Figure 6. Y-Z slices of the dimensionless a) velocity and b) pressure as predicted by the 3-D simulation of a case
 259 with $H/D_0=2$ and $We=40$ ($t/t_{sh}=0.9$).
 260

261 The differences in the shape and breakup modes of the isolated and cluster droplet arrangements are
 262 better explained by looking at Figure 7, which presents the contour of non-dimensional relative
 263 velocity for the same cases as those of Figure 5. In the cluster formation, the air accelerates in the
 264 narrow gap between the droplets (red color in the contour), causing the droplet to deform more at its
 265 periphery rather than its core. This results in the shifting of the breakup mode from multi-bag regime
 266 in the isolated droplet, to shuttlecock in the case of cluster arrangement.
 267



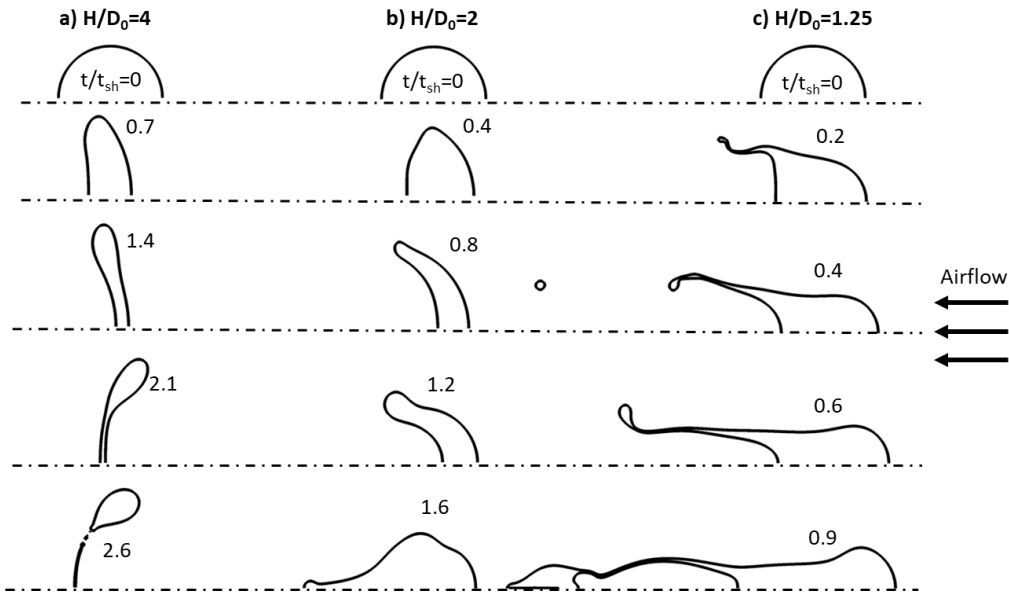
268
 269 Figure 7. Non-dimensional relative velocity contour (X-Z plane) for a case of a droplet in a cluster (3-D and 2-D
 270 axisymmetric) with $We=40$ and $H/D_0=2$, as well as an isolated droplet at the same We number.
 271

272 3.2 Parametric study

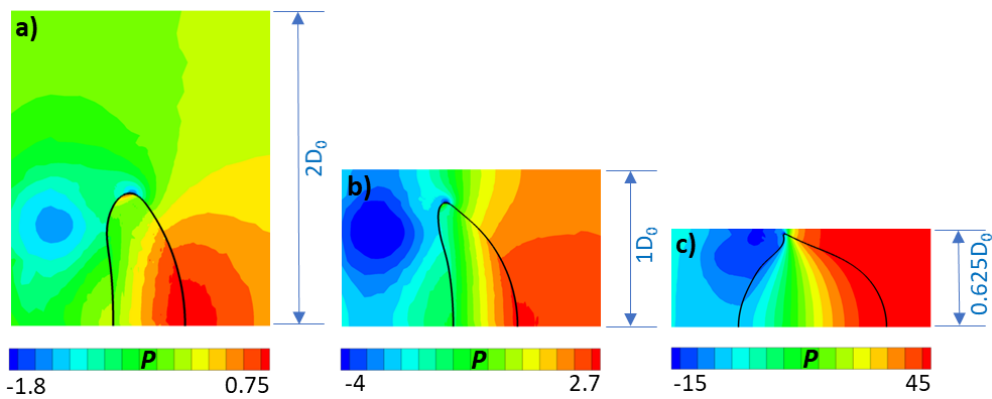
273 3.2.1 Breakup modes

274 In order to investigate the effect of distance between the droplets on the breakup mode, Figure 8
 275 shows the temporal evolution of droplet shape for three cases corresponding to $H/D_0=4$, $H/D_0=2$ and
 276 $H/D_0=1.25$ (2-D axisymmetric domain). For large droplet distances and depending on the We number,
 277 the effect of the surrounding droplets is weak and the breakup mode becomes identical to that of the
 278 isolated droplet (bag breakup mode of Figure 8a). When the distance decreases, the breakup mode
 279 shifts from bag to deformation without breakup (Figure 8b), since the air flow is directed towards the
 280 periphery of the droplet, but without being intense enough to cause liquid stripping from its periphery.
 281 However, when the distance is further decreased, the air velocity becomes high enough to cause the
 282 breakup of the droplet, and the breakup mode shifts to shuttlecock (Figure 8c). This non-monotonic
 283 behaviour is better understood by looking at Figure 9, which presents a highlight of the dimensionless

284 pressure contour $((P - P_\infty)/(\frac{1}{2}\rho_g U_{g,0}^2))$ for the three cases. For the larger droplet distances ($H/D_0=4$
 285 in the figure), the pressure is higher at the core of droplet and lower at its periphery, causing the
 286 formation of the bag. At smaller distances ($H/D_0=2$), the peripheral pressure increases and becomes
 287 equal to the central, therefore preventing the creation of the bag. Finally, at even smaller distances
 288 ($H/D_0=1.25$), the peripheral pressure increases further causing the shuttlecock breakup mode.
 289



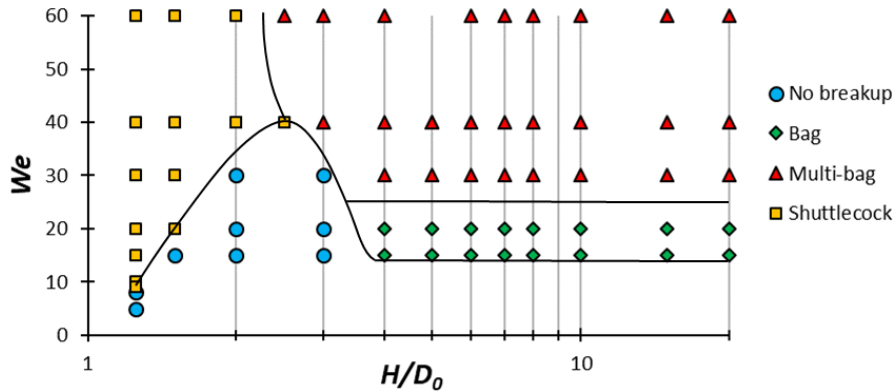
290
 291 Figure 8. Temporal evolution of droplet shape for three cases with $We=15$ and: a) $H/D_0=4$, b) $H/D_0=2$ and c)
 292 $H/D_0=1.25$.
 293



294
 295 Figure 9. Dimensionless pressure contour for three cases with $We=15$ and: a) $H/D_0=4$ ($t/t_{sh}=0.7$), b) $H/D_0=2$
 296 ($t/t_{sh}=0.6$) and c) $H/D_0=1.25$ ($t/t_{sh}=0.1$).
 297

298 The aforementioned observations are summarized in Figure 10, which presents in a H/D_0-We map the
 299 simulated cases of the current work along with the encountered breakup regimes. For $H/D_0 \geq 4$ the
 300 droplets behave as being isolated, i.e. the bag breakup regime is encountered for $We \leq 20$, while for
 301 $We > 20$ they experience the multi-bag mode. For lower values of H/D_0 (< 4) and low We numbers (≤ 30),
 302 the breakup mode shifts to deformation without breakup (Figure 8b). Finally, when the distance
 303 becomes even smaller ($H/D_0 \leq 2.5$), the shuttlecock breakup regime is encountered, even for values of

304 We number as low as 9, which is smaller than the value of the critical We number of an isolated droplet
 305 at the same conditions ($We_{cr,is}=14$).
 306

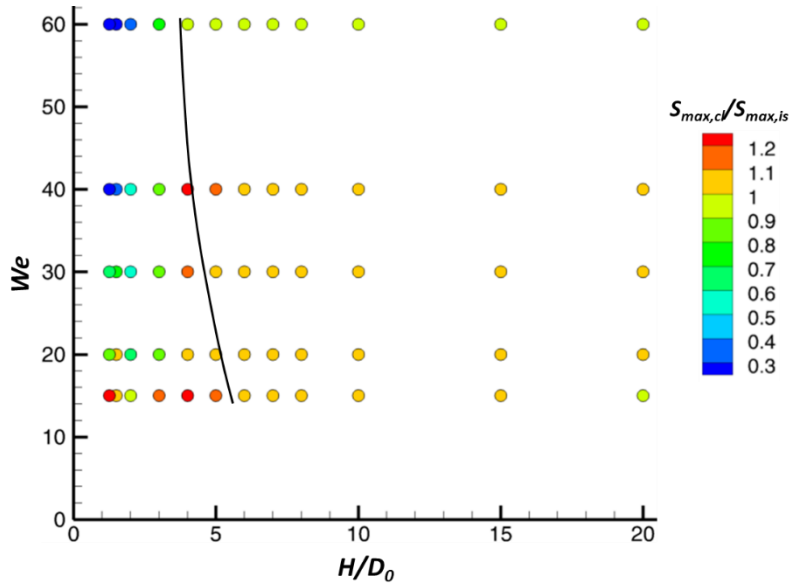


307
 308 Figure 10. H/D_0 - We map with the simulated cases of the current work along with the encountered breakup
 309 regimes ($Oh=0.05$, $\epsilon=51$ and $N=37$).
 310

311 3.2.2 Droplet surface area

312 The droplet surface area is an important quantity for spray applications and is calculated in the CFD
 313 simulations as $S = \sum_i^{n_{cells}} V_{cell} |\nabla a|$, which has been utilized also in [36, 38, 45, 46] and is derived using
 314 the divergence theorem (or Gauss theorem) for the volume fraction at the interface cells. The ratio of
 315 the maximum surface area of a droplet in a parallel moving cluster, to the maximum surface area of
 316 an isolated droplet ($S_{max,cl}/S_{max,is}$) is presented in Figure 11. The ratio $S_{max,cl}/S_{max,is}$ takes very low values
 317 at high We and low H/D_0 , reaching values as low as 0.22, which corresponds to a 78% reduction in the
 318 maximum surface area of a droplet in cluster formation, relative to the one of an isolated droplet at
 319 the same We . This is attributed to the very fast breakup occurring at these conditions, with liquid
 320 stripped from its periphery, while its core remains relatively non-deformed. On the other hand, at low
 321 We and H/D_0 the ratio $S_{max,cl}/S_{max,is}$ is greater than 1, reaching values as high as 1.29, owing to the very
 322 large streamwise droplet deformation (Figure 8c). Finally, the solid line of Figure 11 defines the region
 323 of influence of the maximum surface area of a droplet in cluster formation; this occurs for droplet
 324 distances of approximately $H/D_0 \leq 5$.

325



326

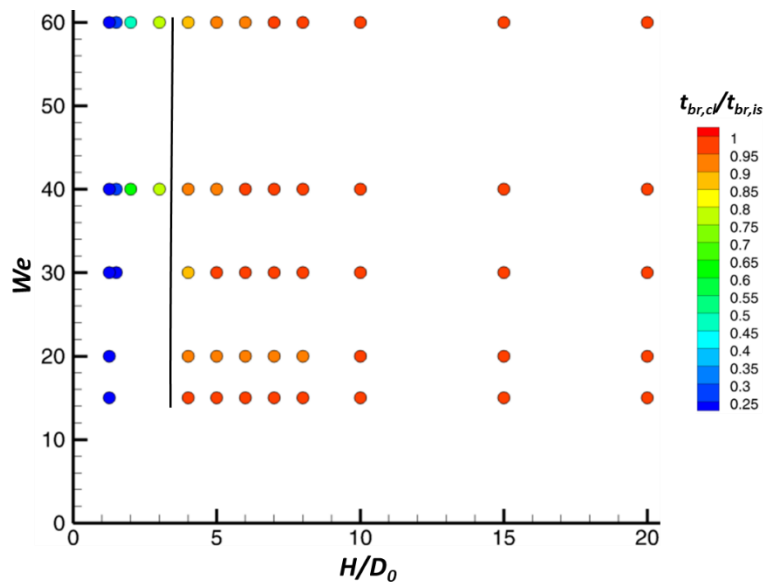
327 Figure 11. Ratio $S_{max,c}/S_{max,is}$ as function of We and H/D_0 . The black line defines the region of influence of the
 328 maximum surface area of a droplet in cluster formation.

329

330 **3.2.3 Breakup initiation time**

331 As already mentioned in Section 3.1, a droplet inside a parallel moving cluster breaks up faster than an
 332 isolated droplet. The breakup initiation time (t_{br}), which is defined as the time instance that a micro-
 333 droplet detaches from the parent droplet for the first time, is measured manually in the simulations
 334 using a visual representation of the process. The ratio $t_{br,c}/t_{br,is}$ is presented in Figure 12 as function of
 335 the We number and the H/D_0 . The ratio $t_{br,c}/t_{br,is}$ decreases with decreasing H/D_0 , reaching values as
 336 low as 0.1. As can be seen from the figure, the breakup time of the cluster formation is different from
 337 that of the isolated at distances $H/D_0 \leq 3$.

338



339

340 Figure 12. Ratio $t_{br,c}/t_{br,is}$ as function of We and H/D_0 . The black line defines the region of influence of the
 341 breakup time of a droplet in cluster formation.

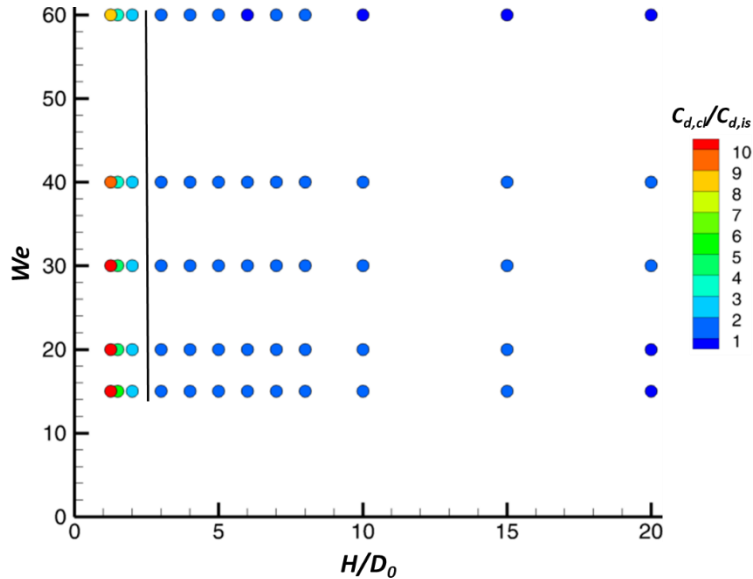
342

343 **3.2.4 Drag coefficient**

344 The drag coefficient (C_d) is calculated using the droplet momentum balance on the droplet with the
 345 effect of virtual mass and Basset forces incorporated into the C_d , similar to previous numerical studies
 346 [47-50]. The effect of droplet frontal area can either i) be incorporated into the drag coefficient and ii)
 347 assumed to vary linearly with time $\frac{A_f(t^*)}{A_{f,0}} = 1 + B \cdot t^*$. The following equations, (3) and (4), are derived
 348 based on the two approaches, respectively, and give the temporal evolution of droplet velocity (their
 349 derivation can be found in our previous work [38]). The average drag coefficient is found for each
 350 simulated case by fitting the equations to the results of the simulations ($U_d - t^*$), as shown in Figure
 351 14 and Figure 13, where the ratios $C_{d,c}/C_{d,is}$ are presented as function of the We number and the H/D_0 ,
 352 using the two approaches. The ratio $C_{d,c}/C_{d,is}$ increases with decreasing H/D_0 , reaching values as high
 353 as 29 for the first approach and 15 for the second one. This trend is in agreement with the works of [1,
 354 15, 17-19]. Overall, the drag coefficient of droplets in cluster formations differs from that of the
 355 isolated droplet for distances $H/D_0 \leq 3$ for the first method, and $H/D_0 \leq 2$ for the second.

$$U_d(t^*) = \frac{U_{g,0}}{\overline{C_d} \left(\frac{3}{4}\right) \left(\frac{1}{\sqrt{\varepsilon}}\right) t^* + 1} \quad (3)$$

$$U_d(t^*) = \frac{U_{g,0}}{\overline{C_d} \left(\frac{3}{4}\right) \left(\frac{1}{\sqrt{\varepsilon}}\right) \left(t^* + \frac{B \cdot (t^*)^2}{2}\right) + 1} \quad (4)$$



360
 361 Figure 13. Ratio $C_{d,c}/C_{d,is}$ as function of We and H/D_0 . The effect of droplet frontal area is incorporated in the
 362 drag coefficient. The black line defines the region of influence of the drag coefficient of a droplet in cluster
 363 formation.
 364

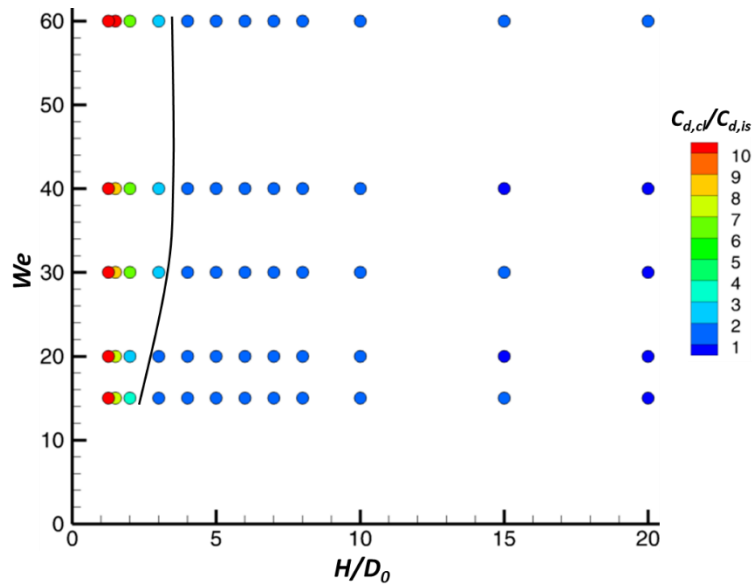


Figure 14. Ratio $C_{d,cl}/C_{d,is}$ as function of We and H/D_0 . The droplet frontal area varies linearly with time. The black line defines the region of influence of the drag coefficient of a droplet in cluster formation.

4 Conclusions

In the current work, 2-D axisymmetric and 3-D simulations were performed with Diesel droplets in a parallel moving cluster. The examined We numbers range from 5 up to 60 and non-dimensional distances between them (H/D_0) from 1.25 up to 20. It was found that for droplet distances $H/D_0 \leq 2.5$ and depending on the We number, the droplets experience the so-called shuttlecock breakup mode, which is characterized by a stretching of the droplet at its periphery, similar to the droplets in tandem formations [4]. This is caused by the high air velocities developed at the gap between the droplets. Furthermore, their breakup occurs faster and experience higher drag coefficients compared to the isolated droplets, effects which are amplified as the distance between the droplets (H/D_0) decreases. At very low droplet distances $H/D_0 < 1.5$, the critical We number of a droplet in a cluster becomes lower than that of an isolated droplet at the same conditions. Overall, it is found that the droplets are affected by the presence of other droplets in the cross-stream direction for distances $H/D_0 \leq 5$.

Acknowledgements

Financial support from the MSCA-ITN-ETN of the European Union's H2020 programme, under REA grant agreement n. 675676 is acknowledged.

References

- [1] Ashgriz, N., 2011, Handbook of atomization and sprays: theory and applications, Springer Science & Business Media.
- [2] Guildenbecher, D. R., López-Rivera, C., and Sojka, P. E., 2009, "Secondary atomization," Experiments in Fluids, 46(3), pp. 371-402.
- [3] Nicholls, J. A., and Ranger, A. A., 1969, "Aerodynamic shattering of liquid drops," AIAA Journal, 7(2), pp. 285-290.
- [4] Stefanitsis, D., Malgarinos, I., Strotos, G., Nikolopoulos, N., Kakaras, E., and Gavaises, M., 2018, "Numerical investigation of the aerodynamic breakup of droplets in tandem," International Journal of Multiphase Flow.
- [5] Temkin, S., and Ecker, G. Z., 1989, "Droplet pair interactions in a shock-wave flow field," Journal of Fluid Mechanics, 202, pp. 467-497.

398 [6] Kékesi, T., Altimira, M., Amberg, G., and Wittberg, L. P., 2019, "Interaction between two deforming liquid drops
399 in tandem and various off-axis arrangements subject to uniform flow," *International Journal of Multiphase Flow*, 112,
400 pp. 193-218.

401 [7] Ozgoren, M., Dogan, S., Canli, E., Akilli, H., and Sahin, B., 2014, "Comparison of Different Configurations of
402 Two Spheres at $Re=5000$ in a Uniform Flow," 17th International Symposium on Applications of Laser Techniques
403 to Fluid Mechanics Lisbon, Portugal.

404 [8] Pinar, E., Sahin, B., Ozgoren, M., and Akilli, H., 2013, "Experimental study of flow structures around side-by-
405 side spheres," *Industrial & Engineering Chemistry Research*, 52(40), pp. 14492-14503.

406 [9] Folkersma, R., Stein, H., and Van de Vosse, F., 2000, "Hydrodynamic interactions between two identical spheres
407 held fixed side by side against a uniform stream directed perpendicular to the line connecting the spheres' centres,"
408 *International Journal of Multiphase Flow*, 26(5), pp. 877-887.

409 [10] Tsuji, T., Narutomi, R., Yokomine, T., Ebara, S., and Shimizu, A., 2003, "Unsteady three-dimensional simulation
410 of interactions between flow and two particles," *International Journal of Multiphase Flow*, 29(9), pp. 1431-1450.

411 [11] Ardekani, A., and Rangel, R., 2006, "Unsteady motion of two solid spheres in Stokes flow," *Physics of Fluids*,
412 18(10), p. 103306.

413 [12] Prahl, L., Hölzer, A., Arlov, D., Revstedt, J., Sommerfeld, M., and Fuchs, L., 2007, "On the interaction between
414 two fixed spherical particles," *International Journal of Multiphase Flow*, 33(7), pp. 707-725.

415 [13] Yoon, D.-H., and Yang, K.-S., 2007, "Flow-induced forces on two nearby spheres," *Physics of Fluids*, 19(9), p.
416 098103.

417 [14] Jadoon, A., Prahl, L., and Revstedt, J., 2010, "Dynamic interaction of fixed dual spheres for several
418 configurations and inflow conditions," *European Journal of Mechanics-B/Fluids*, 29(1), pp. 43-52.

419 [15] Connon, C., and Dunn-Rankin, D., 1996, "Flow behavior near an infinite droplet stream," *Experiments in Fluids*,
420 21(2), pp. 80-86.

421 [16] Zhao, H., Wu, Z., Li, W., Xu, J., and Liu, H., 2019, "Interaction of two drops in the bag breakup regime by a
422 continuous air jet," *Fuel*, 236, pp. 843-850.

423 [17] Kim, I., Elghobashi, S., and Sirignano, W., 1991, "Three-dimensional droplet interactions in dense sprays," 29th
424 Aerospace Sciences Meeting, American Institute of Aeronautics and Astronautics.

425 [18] Kim, I., Elghobashi, S., and Sirignano, W., "Three-dimensional flow computation for two interacting, moving
426 droplets," *Proc. AIAA Materials Specialist Conference-Coating Technology for Aerospace Systems*.

427 [19] Prahl, L., Revstedt, J., and Fuchs, L., "Interaction among droplets in a uniform flow at intermediate Reynolds
428 numbers," *Proc. 44th AIAA Aerospace Sciences Meeting and Exhibit, Reno, Nevada, USA, January*, pp. 9-12.

429 [20] Hirt, C. W., and Nichols, B. D., 1981, "Volume of fluid (VOF) method for the dynamics of free boundaries,"
430 *Journal of Computational Physics*, 39(1), pp. 201-225.

431 [21] Lafaurie, B., Nardone, C., Scardovelli, R., Zaleski, S., and Zanetti, G., 1994, "Modelling Merging and
432 Fragmentation in Multiphase Flows with SURFER," *Journal of Computational Physics*, 113(1), pp. 134-147.

433 [22] "ANSYS®FLUENT, 2014, Release 16.0."

434 [23] Malgarinos, I., Nikolopoulos, N., and Gavaises, M., 2015, "Coupling a local adaptive grid refinement technique
435 with an interface sharpening scheme for the simulation of two-phase flow and free-surface flows using VOF
436 methodology," *Journal of Computational Physics*, 300, pp. 732-753.

437 [24] Strotos, G., Malgarinos, I., Nikolopoulos, N., and Gavaises, M., 2016, "Numerical investigation of aerodynamic
438 droplet breakup in a high temperature gas environment," *Fuel*, 181, pp. 450-462.

439 [25] Malgarinos, I., Nikolopoulos, N., Marengo, M., Antonini, C., and Gavaises, M., 2014, "VOF simulations of the
440 contact angle dynamics during the drop spreading: Standard models and a new wetting force model," *Advances in
441 Colloid and Interface Science*, 212, pp. 1-20.

442 [26] Malgarinos, I., Nikolopoulos, N., and Gavaises, M., 2016, "A numerical study on droplet-particle collision
443 dynamics," *International Journal of Heat and Fluid Flow*, 61, Part B, pp. 499-509.

444 [27] Malgarinos, I., Nikolopoulos, N., and Gavaises, M., 2017, "Numerical investigation of heavy fuel droplet-particle
445 collisions in the injection zone of a Fluid Catalytic Cracking reactor, Part I: Numerical model and 2D simulations,"
446 *Fuel Processing Technology*, 156, pp. 317-330.

447 [28] Malgarinos, I., Nikolopoulos, N., and Gavaises, M., 2017, "Numerical investigation of heavy fuel droplet-particle
448 collisions in the injection zone of a Fluid Catalytic Cracking reactor, part II: 3D simulations," *Fuel Processing
449 Technology*, 156, pp. 43-53.

450 [29] G. Strotos, I. M., N. Nikolopoulos, K. Papadopoulos, A. Theodorakakos, M. Gavaises, 2015, "Performance of
451 VOF methodology in predicting the deformation and breakup of impulsively accelerated droplets," *ICLASS 2015,
452 13th Triennial International Conference on Liquid Atomization and Spray Systems, August 23-27 Tainan, Taiwan*.

453 [30] Strotos, G., Malgarinos, I., Nikolopoulos, N., and Gavaises, M., 2016, "Predicting droplet deformation and
454 breakup for moderate Weber numbers," *International Journal of Multiphase Flow*, 85, pp. 96-109.

455 [31] Strotos, G., Malgarinos, I., Nikolopoulos, N., and Gavaises, M., 2016, "Aerodynamic breakup of an n-decane
456 droplet in a high temperature gas environment," *Fuel*, 185, pp. 370-380.

457 [32] Stefanitsis, D., Malgarinos, I., Strotos, G., Nikolopoulos, N., Kakaras, E., and Gavaises, M., 2017, "Numerical
458 investigation of the aerodynamic breakup of Diesel and heavy fuel oil droplets," *International Journal of Heat and
459 Fluid Flow*, 68, pp. 203-215.

460 [33] Stefanitsis, D., Malgarinos, I., Strotos, G., Nikolopoulos, N., Kakaras, E., and Gavaises, M., 2017, "Numerical
461 investigation of the aerodynamic breakup of Diesel droplets under various gas pressures," 28th Conference on
462 Liquid Atomization and Spray Systems (ILASS-Europe 2017) Valencia, Spain.

463 [34] Stefanitsis, D., Strotos, G., Nikolopoulos, N., Kakaras, E., and Gavaises, M., 2018, "Numerical examination of
464 the aerodynamic breakup of droplets in chain formation," 14th Triennial International Conference on Liquid
465 Atomization and Spray Systems (ICLASS 2018)Chicago, USA.

466 [35] Stefanitsis, D., Strotos, G., Nikolopoulos, N., Kakaras, E., and Gavaises, M., 2019, "Improved droplet breakup
467 models for spray applications," *International Journal of Heat and Fluid Flow*, 76, pp. 274-286.

468 [36] Strotos, G., Malgarinos, I., Nikolopoulos, N., and Gavaises, M., 2016, "Predicting the evaporation rate of
469 stationary droplets with the VOF methodology for a wide range of ambient temperature conditions," *International
470 Journal of Thermal Sciences*, 109, pp. 253-262.

471 [37] Vidal, A., Rodriguez, C., Koukouvinis, P., Gavaises, M., and McHugh, M. A., "Modelling of Diesel fuel properties
472 through its surrogates using Perturbed-Chain, Statistical Associating Fluid Theory," *International Journal of Engine
473 Research*, 0(0), p. 1468087418801712.

474 [38] Stefanitsis, D., Malgarinos, I., Strotos, G., Nikolopoulos, N., Kakaras, E., and Gavaises, M., 2019, "Numerical
475 investigation of the aerodynamic breakup of droplets in tandem," *International Journal of Multiphase Flow*, 113, pp.
476 289-303.

477 [39] Yaws, C. L., and Gabbula, C., 2003, *Yaws" Handbook of Thermodynamic and Physical Properties of Chemical
478 Compounds*, Knovel.

479 [40] Wadhwa, A. R., Magi, V., and Abraham, J., 2007, "Transient deformation and drag of decelerating drops in
480 axisymmetric flows," *Physics of Fluids (1994-present)*, 19(11), p. 113301.

481 [41] Lacaze, G., Misdariis, A., Ruiz, A., and Oefelein, J. C., 2015, "Analysis of high-pressure Diesel fuel injection
482 processes using LES with real-fluid thermodynamics and transport," *Proceedings of the Combustion Institute*, 35(2),
483 pp. 1603-1611.

484 [42] Sutherland, W., 1893, "LII. The viscosity of gases and molecular force," *The London, Edinburgh, and Dublin
485 Philosophical Magazine and Journal of Science*, 36(223), pp. 507-531.

486 [43] Theofanous, T. G., 2011, "Aerobreakup of Newtonian and Viscoelastic Liquids," *Annual Review of Fluid
487 Mechanics*, 43(1), pp. 661-690.

488 [44] Lee, C. H., and Reitz, R. D., 2000, "An experimental study of the effect of gas density on the distortion and
489 breakup mechanism of drops in high speed gas stream," *International Journal of Multiphase Flow*, 26(2), pp. 229-
490 244.

491 [45] Strotos, G., Gavaises, M., Theodorakakos, A., and Bergeles, G., 2008, "Numerical investigation on the
492 evaporation of droplets depositing on heated surfaces at low Weber numbers," *International Journal of Heat and
493 Mass Transfer*, 51(7-8), pp. 1516-1529.

494 [46] Strotos, G., Gavaises, M., Theodorakakos, A., and Bergeles, G., 2011, "Numerical investigation of the
495 evaporation of two-component droplets," *Fuel*, 90(4), pp. 1492-1507.

496 [47] Quan, S., and Schmidt, D. P., 2006, "Direct numerical study of a liquid droplet impulsively accelerated by
497 gaseous flow," *Physics of Fluids (1994-present)*, 18(10), p. 102103.

498 [48] Khare P., V. Y., "Drag Coefficients of Deforming and Fragmenting Liquid Droplets," *Proc. ICLASS Americas,
499 25th Annual Conference on Liquid Atomization and Spray Systems*.

500 [49] Yang, W., Jia, M., Sun, K., and Wang, T., 2016, "Influence of density ratio on the secondary atomization of
501 liquid droplets under highly unstable conditions," *Fuel*, 174, pp. 25-35.

502 [50] Shao, C., Luo, K., and Fan, J., 2017, "Detailed numerical simulation of unsteady drag coefficient of deformable
503 droplet," *Chemical Engineering Journal*, 308, pp. 619-631.

504

505